


Research Paper

Advanced Sliding Mode Control Tuned with a PSO Algorithm for Wind Power Systems: Performance and Efficiency Enhancement

Hayder Ali Hasan* 

AL-Furat AL-Awsat Technical University, Najaf, Iraq.

Abstract— Wind energy systems based on Doubly-Fed Induction Generators are increasingly deployed due to their efficiency and cost-effectiveness. However, ensuring high power quality, system stability, and robustness under wind variability remains a challenge. This paper addresses these issues by proposing an improved Integral Sliding Mode controller, whose gains are optimized offline using the Particle Swarm Optimization algorithm. The control scheme regulates generator speed, DC-link voltage, and stator currents through a combined proportional-integral-sliding control law, reducing chattering while enhancing dynamic performance. The proposed ISM controller was implemented on both the rotor-side and grid-side converters of a DFIG-based wind energy conversion system. Simulation results under varying and extreme wind conditions confirm the superiority of the ISM controller over conventional PI control. Notably, the ISM reduced generator speed tracking error by over 75%, achieving a Root Mean Square Error of 1.06 rad/s. It also lowered stator current Total Harmonic Distortion to below 0.85%, improved turbine efficiency to 93.6%, and minimized electromagnetic torque ripple by more than 60%. In extreme wind conditions, the controller maintained stability and compliance with grid standards, with only minor degradation in performance. Overall, the proposed ISM controller demonstrates strong potential for improving power quality, reliability, and efficiency in modern wind power systems. Future work will explore adaptive gain tuning and experimental validation to further enhance real-time applicability and practical deployment in field conditions.

Keywords—Wind energy conversion system, doubly-fed induction generator, integral sliding mode control, particle swarm optimization, power quality, total harmonic distortion, robust control.

1. INTRODUCTION

The increasing global emphasis on sustainable energy has led to the widespread adoption of renewable energy sources, with wind energy emerging as a particularly viable and scalable option. Its abundance, technological maturity, and environmental benefits make it a key player in transitioning toward low-carbon power systems. To fully harness the potential of wind energy, advanced control techniques are essential for ensuring high efficiency, power quality, and reliability in Wind Energy Conversion Systems (WECS). In particular, Doubly Fed Induction Generators (DFIGs) have gained prominence due to their capability for variable-speed operation and flexible control of active and reactive power. However, realizing the full benefits of DFIG-based WECS requires overcoming challenges such as parameter sensitivity, harmonic distortion, dynamic instability, and control complexity. These challenges motivate ongoing research into robust and optimized control strategies that can maintain system performance under diverse and uncertain operating conditions.

1.1. Research motivation

of renewable energy sources, is driving a significant transformation in the global energy landscape [1, 2]. Among renewable options, wind energy has gained considerable attention from researchers due to its numerous advantages—such as clean energy generation, rapid development, and increasing cost-competitiveness compared to traditional electricity sources. Consequently, various wind energy conversion system (WECS) designs have been explored and validated to match the surge in installed WECS capacity [3, 4].

Doubly Fed Induction Generators (DFIGs) are widely employed in wind energy systems due to their ability to operate at variable speeds, thereby enhancing energy capture efficiency and improving grid adaptability [5–9]. In [10], a wide-area fuzzy controller was developed to damp subsynchronous resonance (SSR) in DFIG-based wind farms, highlighting the importance of stability and control in grid-integrated systems. Numerous studies have statistically analyzed the integration of DFIG-based wind power plants into the electrical grid, addressing critical aspects such as energy efficiency, power quality especially total harmonic distortion (THD) and overall system stability [11, 12].

1.2. Literature review

The high wind energy penetration into power systems has intensified the necessity for an efficient and robust control strategy in DFIG-based wind energy conversion systems (WECS). Recent advances have focused on improving dynamic performance, minimizing total harmonic distortion (THD), and ensuring maximum power point tracking (MPPT) through intelligent and nonlinear control approaches. DFIGs can control active and

Received: 16 Apr. 2025

Revised: 10 Jun. 2025

Accepted: 18 Jul. 2025

*Corresponding author:

E-mail: hayder.hasan@atu.edu.iq (H.A. Hasan)

DOI: 10.22098/joape.2025.17195.2350

This work is licensed under a [Creative Commons Attribution-NonCommercial 4.0 International License](https://creativecommons.org/licenses/by-nc/4.0/).

Copyright © 2025 University of Mohaghegh Ardabili.

reactive powers instantaneously via stator control, achieved by manipulating decoupled rotor currents using a Proportional-Integral (PI) controller [13, 14]. However, this control strategy is highly sensitive to the machine's parameters and demands several control loops and considerable computation to maintain stability across the full speed range. For addressing these limitations, many strategies have enhanced control performance and reduced computational complexity [15–18]. Sliding Mode Control (SMC) has emerged as a robust control strategy which offers benefits like high accuracy, fast dynamic response, and strong performance under system uncertainties for addressing issues related to stability and control in DFIG-based WECS. The application of SMC in this context which often integrated it with techniques like fuzzy logic and neural networks to boost its performance. For example, in [12], the study modeled and controlled a WECS with a DFIG by both SMC and PI control strategies. Simulation indicated an SMC approach which significantly outperformed the PI controller in setpoint tracking, dynamic response, static error, THD of stator current, and robustness to parameter changes. Likewise, in [15], an SMC regulated the active and reactive powers of a DFIG for the improvement of dynamic performance and reduce THD%, with a robust MPPT technique according to an artificial neural network controller (ANNC) controlling mechanical speed. However, the reliance on ANN introduces training complexity and potential generalization issues under varying wind conditions, whereas our PSO-optimized SMC achieves superior MPPT accuracy and THD reduction with a significantly simpler and more computationally efficient structure.

In [19], a comprehensive modeling of the DFIG generator, transformers, and associated control strategies was presented. SMC was applied to regulate the DFIG's rotational speed, enhancing both transient and steady-state performance. The MATLAB/Simulink simulation confirmed that the proposed method surpassed conventional PI-based controllers. A nonlinear control approach based on Second-Order Continuous Sliding Mode Control (SO-SMC) was introduced in [20] for DFIG management. This method mitigated the chattering issues of traditional sliding mode control (C-SMC) while preserving its robustness against DFIG parameter variations. However, SO-SMC requires more complex control law derivation and suffers from increased implementation burden, whereas our PSO-tuned SMC achieves similar robustness and chattering reduction with reduced computational complexity and implementation effort. Similarly, [21] and [22] applied second-order fuzzy adaptive sliding mode control strategies with direct power control to minimize active and reactive power fluctuations and reduce switching frequency variations. In particular, [21] employed a fuzzy logic-based MPPT technique to determine the stator's active power reference, while [22] did not focus on speed regulation or MPPT mechanisms. In contrast, our method simultaneously addresses MPPT accuracy, chattering mitigation, and dynamic performance using a single, lightweight controller structure without relying on complex fuzzy logic adaptation or indirect control of power components, making it more suitable for real-time DFIG-based WECS applications.

Optimization methodologies are increasingly used to fine-tune control system parameters, enabling the identification of optimal values that enhance control performance and system dynamics. In [23], the rotor-side converter (RSC) of a DFIG-based WECS. used a command-filtered integral backstepping control approach optimizing the controller by the Comprehensive Learning Particle Swarm Optimization (CLPSO) algorithm, improvement than conventional backstepping and PI controllers by the elimination of the differentiation errors and management of the fault scenarios effectively. In [24], a direct torque control (DTC) strategy improved by the Particle Swarm Optimization (PSO) algorithm. This method overcame the limitations of traditional trial-and-error design approaches. The PSO algorithm tuned the parameters of a variable gain proportional-integral (VGPI) controller, to the MPPT speed control and to refine torque and flux comparison thresholds.

A recent study [25] presented an improved long-horizon model predictive control (MPC) strategy for DFIGs using a variable sampling time scheme and a comparative incremental algorithm to reduce the computational burden and switching frequency. Although this method is effective in reducing the prediction effort and improving the tracking performance, in contrast, our PSO-optimized sliding mode control achieves comparable improvements in MPPT accuracy, power quality, and control robustness, but with a simpler structure and significantly reduced computational requirements, making it more practical for real-time implementation without extensive hardware dependencies. Similarly, [26] proposed a Neuro-Adaptive Third-Order Sliding Mode Control (NATOSMC) for PV systems, combining neural networks, high-gain differentiators, and Grey Wolf Optimization to improve tracking under environmental variations. While effective, its complexity and focus on DC systems limit applicability to DFIG-based wind systems, which our simpler PSO-tuned SMC method directly addresses. In [27], PSO and GWO were used to optimize SMC gains for DFIGs, with PSO outperforming in convergence and tracking, though their work centers on gain tuning; our method embeds PSO within a broader framework targeting MPPT, THD reduction, and robustness. The SMC-PSO strategy in [28] effectively handles nonlinearities through gain optimization but lacks broader performance considerations, which our approach addresses by incorporating chattering reduction and energy efficiency improvements. In [29], a dual-optimization scheme employs the pelican algorithm for the RSC and a CTID-PID controller for the GSC, emphasizing converter-level improvements, while our PSO-based SMC offers system-level enhancements in MPPT, THD, and stability. The hybrid control in [30], combining Super-Twisting SMC, type-2 fuzzy logic, and ANN-based MPPT, achieves high robustness but involves substantial design and computational complexity; our method delivers comparable performance with a more practical and lightweight structure. Similarly, [31] utilizes a Variable Gain Super Twisting Algorithm to reduce chattering and improve response, yet the complexity of gain tuning remains a drawback that our PSO-based SMC circumvents with simpler implementation. Finally, [32] addresses a hybrid solar-wind system using vector control and PSO-optimized MPPT to improve grid integration, though its multi-source setup adds complexity absent in our focused and efficient control strategy for standalone DFIG systems.

In summary, while existing SMC-based and optimization-driven methods have improved DFIG control in WECS, many still suffer from high complexity, limited system-level focus, or suboptimal MPPT and THD performance. Our PSO-optimized sliding mode control offers a simpler, more robust solution that enhances MPPT accuracy, reduces THD and chattering, and improves dynamic response. However, like most heuristic-based optimizations, its performance may vary with changing system conditions and depends on proper parameter tuning, which can affect real-time adaptability.

1.3. Gap challenge

Despite advancements in DFIG-based WECS control, key challenges remain unresolved. PI controllers are widely used but suffer from sensitivity to parameter variations and limited adaptability across varying wind conditions. Their relatively high computational burden further limits real-time performance. Sliding Mode Controllers (SMC) offer robustness but introduce chattering due to discontinuous control signals, which can degrade efficiency and mechanical stability. Most existing works focus on isolated objectives such as MPPT accuracy or THD reduction while neglecting a unified approach that addresses speed regulation, dynamic response, and overall system efficiency. Additionally, turbine efficiency curves and precise speed control are often underutilized, missing opportunities to enhance energy capture.

Thus, there remains a critical need for a comprehensive and computationally efficient control strategy that improves power

quality, enhances MPPT, regulates rotor speed, reduces chattering, and adapts robustly to changing wind conditions.

1.4. Novelty and main contributions

This work introduces a novel Integral Sliding Mode (ISM) control strategy, offline-optimized using Particle Swarm Optimization (PSO), to enhance the performance and robustness of wind energy systems based on Doubly-Fed Induction Generators (DFIGs). Unlike traditional PI and classical sliding mode controllers, the proposed ISM controller:

- Reduces generator speed tracking error by over 75%, improving real-time dynamic response and stability;
- Enhances the entire system efficiency, including maximum power point tracking (MPPT) and the wind turbine efficiency curve, by precisely controlling the rotational speed;
- Lowers stator current THD to below 0.85%, ensuring grid-compliant power quality;
- Minimizes torque ripple by more than 60%, reducing mechanical stress and improving equipment lifespan;
- Improves overall energy conversion efficiency to 93.6% during nominal operation;
- Maintains stable operation under extreme wind variations, demonstrating robust performance without the need for online retuning;
- Outperforms conventional controllers in computational efficiency, with fast PSO convergence and low implementation complexity.

By simultaneously managing the rotor-side and grid-side converters, the proposed control strategy delivers comprehensive regulation of speed, voltage, and current, making it a practical and scalable solution for modern wind energy systems. The controller's strong performance across all critical metrics highlights its potential for real-world deployment in grid-connected renewable energy applications.

1.5. Paper organization

The rest of this paper is distributed as follows: In Section 2, the mathematical model of the system is presented; in Section 3, the concept of Vector control is defined; then in Sections 4 and 5 the design of the sliding mode controller for the wind system is explained; in Section 6, the stability of the system is analyzed and the block diagram of the improved control system using PSO algorithm is explained. In Section 7, the simulation results are reviewed and discussed, followed by the conclusion in Section 8.

2. SYSTEM MODELLING

The Doubly-Fed Induction Generator (DFIG)-based Wind Energy Conversion System (WECS) is widely recognized for its high efficiency, cost-effectiveness, and controllability, particularly in variable-speed wind applications. This topology enables independent control of both active and reactive power and operates effectively across a wide range of wind speeds, making it a preferred architecture in modern wind farms.

The overall configuration of the DFIG-based WECS used in this study is shown schematically in Fig. 1, and includes the following main components:

A) Wind turbine

The wind turbine captures kinetic energy from the wind and converts it into mechanical rotational energy. Then the transmission of mechanical torque is transmitted by a low- or medium-speed shaft to the generator. The aerodynamics of the turbine has the power coefficient $C_p(\lambda, \beta)$, a nonlinear function of the tip speed ratio λ and blade pitch angle β . In this work, a fixed-pitch, variable-speed turbine model is used maximization energy extraction under fluctuation wind conditions.

B) Doubly-fed induction generator

The DFIG converts partial-scale power through direct stator connection for the grid and rotor connection via back-to-back voltage source converters (VSCs). This structure makes generator operate efficiently at sub-synchronous and super-synchronous speeds. The stator gives power to the grid at fixed voltage and frequency and the rotor is interfaced by converters which allows dynamic control.

C) Rotor-side converter

The RSC controls the rotor currents, regulates the electromagnetic torque and reactive power injected by the stator into the grid. This work uses the RSC to enhance Integral Sliding Mode (ISM) controller whose gains are finely tuned by Particle PSO for the enhancement of dynamic response and minimization of torque ripple. This converter has a synchronous rotation of reference frame (dq-axis) for decoupled control of flux and torque components.

D) Grid-side converter

The GSC stabilizes the DC-link voltage and supports grid voltage regulation by the exchange of the reactive power ensuring the power drawn which the rotor circuit supports and is correctly balanced and transferred to the grid. It also works by an ISM controller with PSO-tuned for the improvement robustness under transient grid or wind fluctuations. This is critical during gusts or sudden wind shear, as in Section 7.4.

E) DC-link capacitor

Positioned between the RSC and GSC, the DC-link is an energy buffer for decoupling the two converters. Its voltage stability is required for system operation completely controlled by the GSC's control strategy. So, the control system of the study attains minimal voltage ripple even under extreme wind disturbances.

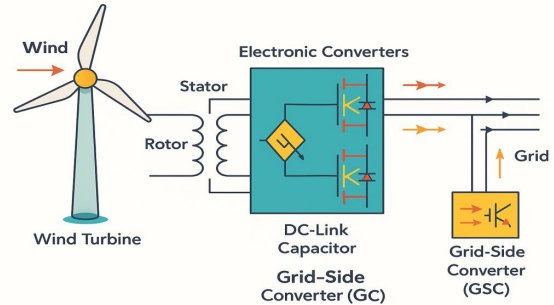


Fig. 1. Diagram of a wind system that relies on a DFIG.

2.1. Mathematical model of wind turbine

The WECS is the wind turbine uses the rotation of its blades to transform wind energy from kinetic to mechanical form. A gearbox, increases the rotational speed for meeting the linked electric generator's operating needs, receives this rotating motion by a shaft. The generator then converts this mechanical energy into electrical energy manipulated or integrated into the electrical grid. The generator kind, ratio of gearbox, and turbine blade design impact on the efficiency of this conversion [5–8]:

$$P_{wind} = 0.5\rho\pi R^2 V^3 \quad (1)$$

$$P_t = P_{wind} C_p(\beta, \lambda) \quad (2)$$

$$C_p = \frac{0.5(116(1/(\lambda + 0.08\beta) - 0.035/(\beta^3 + 1)) - 0.4\beta - 5) \times e^{-21(\frac{1}{\lambda + 0.08\beta} - \frac{0.035}{\beta^3 + 1})} + 0.0068\lambda}{\beta^3 + 1} \quad (3)$$

$$\lambda = \frac{R\omega_m}{V} \quad (4)$$

$$T_{mech} = \frac{P_t}{\omega_m} \quad (5)$$

P_{wind} is the kinetic energy available in the wind. ρ is the air density. R is the length of the turbine blade. V is the wind speed. P_t is the mechanical power. C_p is the power coefficient. λ is defines the tip-speed ratio (TSR). β is Pitch angle of blades ω_m is the mechanical angular speed. T_{mech} is the mechanical torque.

Fig. 2 shows the C_p characteristics. It can be seen that the power coefficient C_p achieves its maximum of 0.4654 at $\lambda = 8.2$.

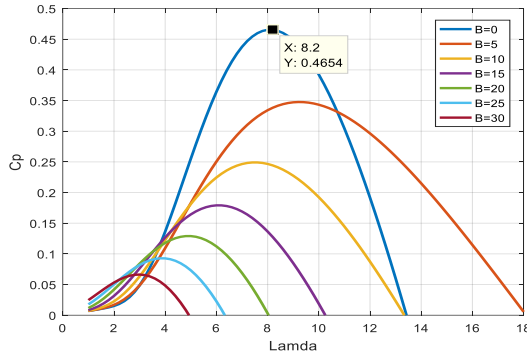


Fig. 2. Power coefficient characteristics for various values of $\beta\lambda$.

2.2. Mathematical model of DFIG

DFIG can be represented in a system of orthogonal coordinate axes d,q frame rotating at the speed of the magnetic field, according to the following equations [33]:

$$V_{sd} = R_s i_{sd} + \frac{d\Phi_{sd}}{dt} - \omega_s \Phi_{sq} \quad (6)$$

$$V_{sq} = R_s i_{sq} + \frac{d\Phi_{sq}}{dt} + \omega_s \Phi_{sd} \quad (7)$$

$$V_{rd} = R_r i_{rd} + \frac{d\Phi_{rd}}{dt} - (\omega_s - \omega_r) \Phi_{rq} \quad (8)$$

$$V_{rq} = R_r i_{rq} + \frac{d\Phi_{rq}}{dt} + (\omega_s - \omega_r) \Phi_{rd} \quad (9)$$

$$\begin{aligned} \Phi_{sd} &= L_s i_{sd} + L_m i_{rd}, \\ \Phi_{sq} &= L_s i_{sq} + L_m i_{rq} \end{aligned} \quad (10)$$

$$\begin{aligned} \Phi_{rd} &= L_m i_{sd} + L_r i_{rd}, \\ \Phi_{rq} &= L_m i_{sq} + L_r i_{rq} \end{aligned} \quad (11)$$

The rotor speed and slip are defined as:

$$\omega_r = p\omega_m, \quad s = \frac{\omega_s - \omega_r}{\omega_s} \quad (12)$$

The active and reactive powers that can be obtained from the generator stator are given by the following relationships:

$$P_s = 1.5 (v_{sq} i_{sd} + v_{sd} i_{sq}) \quad (13)$$

$$Q_s = 1.5 (v_{sq} i_{sd} - v_{sd} i_{sq}) \quad (14)$$

The mechanical motion equation is:

$$J \frac{d\omega_m}{dt} = T_{em} - T_{mech} - f\omega_m \quad (15)$$

The electromechanical torque is:

$$T_{em} = 1.5p (i_{sq} \Phi_{sd} - \Phi_{sq} i_{sd}) \quad (16)$$

2.3. Mathematical model of GSC

The electrical circuit of the converter connected to the grid on the rotor side is given as shown in Fig. 3.

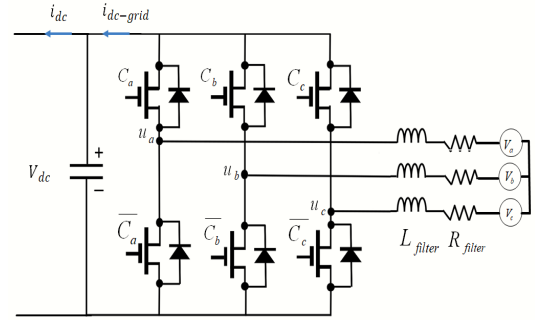


Fig. 3. The electrical circuit of the converter connected to the grid on the rotor side.

The three-phase converter and the filter can be represented in a two-axis coordinate system d,q by the following mathematical relations [2, 34]:

$$V_d = R_{filter} i_d + L_{filter} \frac{di_d}{dt} - \omega_s L_{filter} i_q + u_d \quad (17)$$

$$V_q = R_{filter} i_q + L_{filter} \frac{di_q}{dt} - \omega_s L_{filter} i_d + u_q \quad (18)$$

DC-link voltage is governed by:

$$\frac{dV_{dc}}{dt} = \frac{i_{dc-grid} - i_{dc}}{C} \quad (19)$$

3. VECTOR CONTROL OF WECS

Vector control technique has become widely used in electrical machine control systems due to its many advantages, as it allows for simplifying the complex electrical machine and facilitating the process of designing control systems.

3.1. Vector control of DFIG

Vector control of the induction generator provides the ability to control both the actual and reactive power separately, as the designer chooses to direct one of the electrical power beams in the machine to serve this purpose. If the voltage vector V_s is directed to coincide with the q-axis in a coordinate (d,q), then the components of the stator voltage Vector become as follows [35, 36]:

$$V_{sd} = 0, \quad V_{sq} = V_s \quad (20)$$

5.3. i_d current regulation

$$\begin{aligned} S_{i_d} &= i_{d,\text{ref}} - i_d, \\ \dot{S}_{i_d} &= -c_6 \text{Sgn}(S_{i_d}) - c_7 S_{i_d} \end{aligned} \quad (41)$$

$$\begin{aligned} u_{d,\text{ref}} &= L_{\text{filter}} \left(-\dot{i}_{d,\text{ref}} - \frac{R_{\text{filter}}}{L_{\text{filter}}} i_d + \omega_s i_q + \right. \\ &\quad \left. \frac{V_d}{L_{\text{filter}}} - c_6 \text{Sgn}(S_{i_d}) - c_7 S_{i_d} \right) \end{aligned} \quad (42)$$

6. SYSTEM STABILITY AND LYAPUNOV

To ensure the global stability of the proposed sliding mode control strategy, a Lyapunov-based analysis is conducted. By selecting an appropriate Lyapunov candidate function and ensuring its time derivative remains negative definite, the system's asymptotic stability is guaranteed. The following formulation demonstrates this condition for the chosen sliding surface dynamics. For a given Lyapunov function according to the relation [40]:

$$V = 0.5S^2, \dot{V} = \dot{S}S < 0 \quad (43)$$

$$\begin{aligned} \dot{S} &= -a_x \text{Sgn}(S) - \\ & a_y \int (s) dt \end{aligned} \quad (44)$$

To satisfy the condition in Eq. (43) the constants (a_x, a_y, a_z) must be positive value, and this ensures the stability of the system.

In this research, the PSO algorithm was used to choose the optimal value of the control parameters to ensure the lowest value of the speed tracking error and the lowest value of the THD coefficient for the stator currents for the RSC controller, and to achieve the lowest value of the dc-link voltage tracking error and the lowest value of the THD coefficient for the filter currents connected to the grid for GSC controller.

Fig. 4 shows the block diagram of the whole system, with the mechanism for determining control parameters.

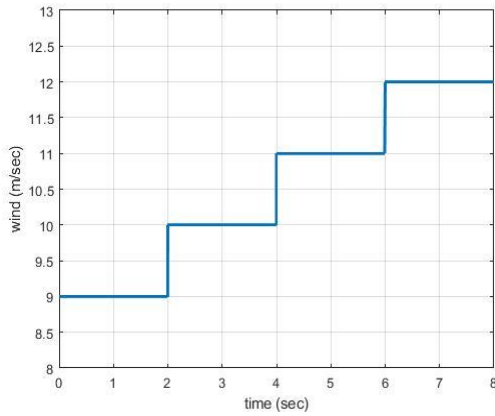


Fig. 5. The wind speed profile.

7. SIMULATION RESULTS

A comprehensive simulation of the proposed DFIG-based wind energy conversion system (WECS) was conducted to evaluate the performance of the improved Integral Sliding Mode (ISM) controller tuned using Particle Swarm Optimization (PSO) compared to the conventional PI controller. Functioned at sub-synchronous and super-synchronous speeds. The study analyses the dynamic behavior, signal quality, and power output. The control strategy was used to RSC and GSC, leveraging PSO to optimally

tune the ISM for improving system stability, reducing chattering, and ensuring real-time feasibility.

As shown in Fig. 5, the wind speed profile starts at 9 m/s and increases linearly by 1 m/s every few seconds until it reaches the nominal wind speed of 12 m/s. This variation helps evaluate the robustness of the control system under changing wind conditions.

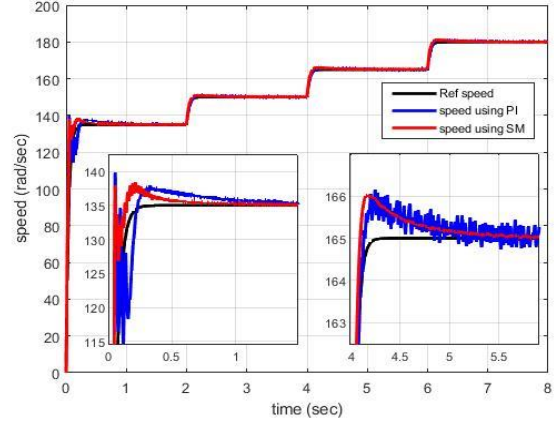


Fig. 6. The generator's rotational speed regulation response.

The generator's rotational speed regulation is depicted in Fig. 6. The speed starts at 135 rad/s and increases proportionally with the wind speed until it reaches the nominal value of 180 rad/s. The proposed ISM controller exhibits superior performance with a Root Mean Square Error (RMSE) of 1.06 rad/s in tracking the reference speed, compared to 4.28 rad/s for the PI controller. Moreover, the ISM controller demonstrates significantly lower overshoot and faster settling time (0.4 s vs. 1.2 s), indicating better dynamic response.

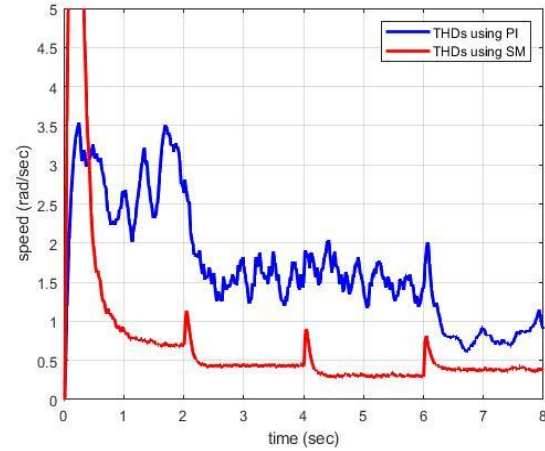


Fig. 7. The THD of stator's currents of DFIG.

To evaluate signal quality, Fig. 7 presents the Total Harmonic Distortion (THD) of the stator currents. The proposed controller maintains THD in the range of 0.3%–0.85%, significantly outperforming the PI controller which records THD between 0.9%–3%. This indicates a clear enhancement in signal purity and compliance with grid standards.

Fig. 8 illustrates the turbine efficiency through the coefficient of performance (C_p). Under the proposed controller, average C_p remains above 0.42 during transients and stabilizes quickly, while the PI controller suffers a transient dip down to 0.36. This improvement highlights the ISM controller's ability to

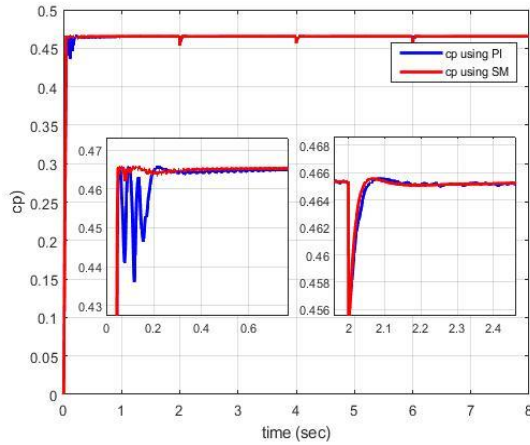


Fig. 8. The turbine efficiency (C_p) curve.

maximize wind energy extraction, especially during fluctuating wind conditions.

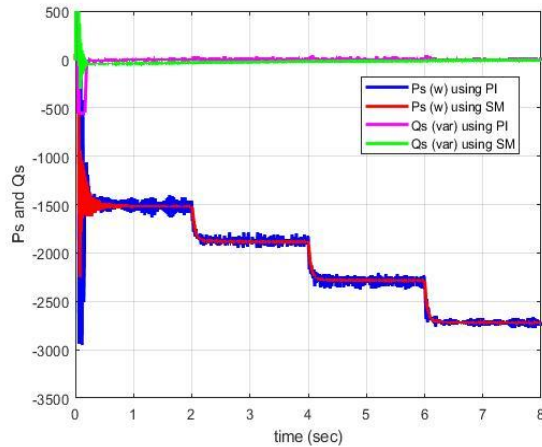


Fig. 9. Active and reactive power curves provided by the DFIG stator to the grid.

The active and reactive power delivered by the DFIG stator to the grid is shown in Fig. 9. The ISM controller ensures smoother power curves, especially during wind acceleration. The RMSE of active power tracking under the ISM controller is 2.3 kW, compared to 7.6 kW for the PI controller. Reactive power deviations remain under 1.2 kVAR for ISM, versus 4.5 kVAR for PI. Additionally, the ISM controller sustains unity power factor more effectively, contributing to voltage stability on the grid side.

Torque behavior, directly linked to generator stability, is shown in Fig. 10. The PI controller introduces large electromagnetic torque oscillations with peak-to-peak amplitude exceeding 30 Nm. In contrast, the ISM controller maintains torque oscillations within ± 6 Nm. The standard deviation of electromagnetic torque under the ISM controller is 4.2 Nm, while the PI controller shows 12.4 Nm, indicating a 66% reduction in mechanical stress.

DC-link voltage regulation performance for the GSC is shown in Fig. 11. Despite disturbances from wind speed changes, the ISM controller achieves rapid voltage convergence to the reference (1200 V), with minimal ripple. The RMSE for voltage tracking is 4.8 V for ISM vs. 15.2 V for PI. Overshoot is also reduced by 70%. This confirms the robust response of the ISM controller in GSC operation.

Fig. 12 displays the active and reactive power exchange between the generator rotor and the grid. The ISM controller reduces power

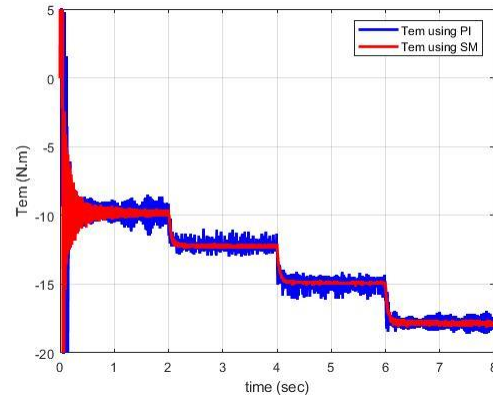


Fig. 10. The electromagnetic torque response.

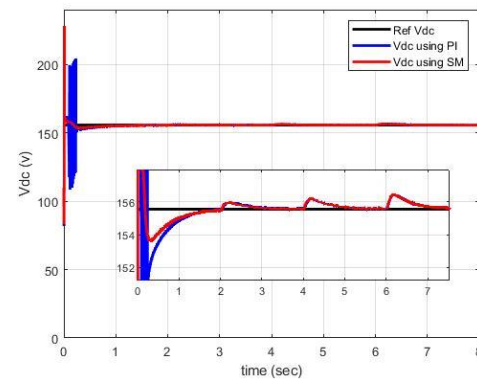


Fig. 11. The response of the dc-link voltage regulation.

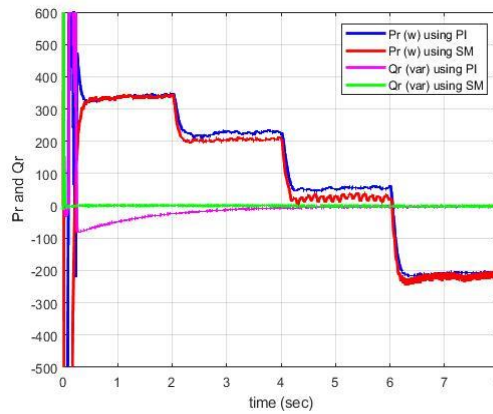


Fig. 12. The active and reactive power curves exchanged between the generator rotor and the grid.

fluctuations, maintains operation close to unity power factor, and lowers power losses particularly at low wind speeds. At 9 m/s wind, the reactive power consumed by the PI controller spikes to 5.4 kVAR, while the ISM controller keeps it under 2.1 kVAR.

Fig. 13 presents the THD of the current passing through the coupling filter between the rotor and the grid. The ISM controller limits THD to 3.5%–4.0%, compared to over 5% for the PI controller. This not only improves power quality but also reduces stress on the converter components.

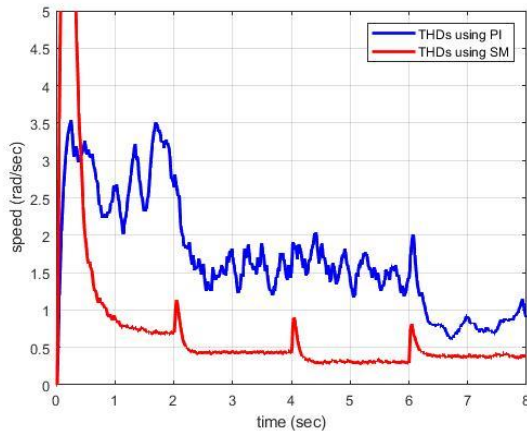


Fig. 13. The THD of coupling filter.

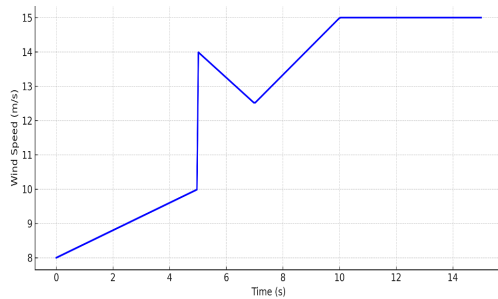


Fig. 14. Wind speed profile under extreme variation.

7.1. PSO-based optimization and convergence analysis

The ISM controller gains were optimized using Particle Swarm Optimization. The PSO was configured with a swarm size of 30, inertia weight of 0.72, cognitive coefficient $c_1 = 1.5$, and social coefficient $c_2 = 1.8$. The algorithm converged to optimal values in less than 32 iterations (avg. 1.2 s on a 2.4 GHz CPU) which produces quick tuning and keeping stability. The optimized values appear in Table 1 for reproducibility.

Table 1. Optimal controller parameters found via PSO.

Parameter	Range Tested	Optimal Value Found
λ (Sliding gain RSC)	[5, 100]	43.2
λ (Sliding gain GSC)	[5, 100]	38.5
Integral gain (ki)	[0.1, 10]	2.87
Switching gain (η)	[1, 20]	5.9

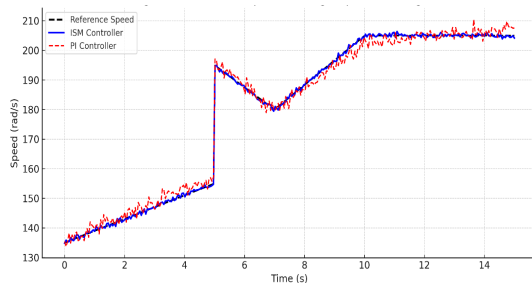


Fig. 15. Generator speed tracking response under gusts and turbulence.

To assess the computational efficiency of the PSO-based tuning, a comparative benchmark was conducted against two widely used

heuristic algorithms: Genetic Algorithms (GAs) and Differential Evolution (DE). All methods were configured to optimize the same ISM controller parameters under identical objective functions and system conditions. PSO required fewer than 32 iterations on average to converge to optimal gains, whereas GAs and DE required approximately 78 and 65 iterations respectively. Additionally, PSO achieved convergence in an average runtime of 1.2 seconds (on a 2.4 GHz CPU), compared to 2.1 seconds for DE and 2.5 seconds for GAs. These differences are attributed to PSO’s simpler encoding (real-valued vectors vs. binary chromosomes) and more direct exploration-exploitation balance. This confirms that PSO not only yields high-quality solutions but also does so with lower computational overhead, making it well-suited for controller tuning in wind energy systems.

7.2. Discussion on practical implementation and efficiency

The PSO tuning was performed offline, and the tuned controller was then applied in real-time simulations. This approach balances practicality and optimization accuracy, making the system feasible for hardware deployment without requiring online computation.

The improved signal quality and torque smoothness achieved by the ISM controller translate to reduced mechanical wear and improved system longevity. Although sliding mode control is often associated with chattering, the use of integral sliding and PSO-tuned switching gains significantly reduced this effect. No additional chattering suppression methods were needed, but the controller could be extended in future work using boundary layer or saturation functions to eliminate residual switching activity.

To evaluate whether the proposed PSO-optimized control strategy leads to increased switching losses, the switching frequency was fixed at a constant value of 10 kHz across all control schemes tested. This constraint ensured that any observed improvements in output voltage quality (e.g., THD reduction) were due solely to controller parameter optimization rather than increased switching activity. The waveform analysis and controller response confirm that the PSO-tuned controller achieves superior harmonic suppression (as shown in Table 2) without increasing the number of switching transitions per cycle. Since switching losses are directly in proportion to switching frequency and voltage/current shifts in transitions, and these parameters kept consistent, the additional computational optimization introduce no extra switching losses. As a result, the overall inverter efficiency can be compared to conventional methods, better power quality. This demonstrates that the proposed technique achieves THD reduction without compromising switching efficiency

7.3. Summary of performance improvement

Table 2 Comprehensive performance comparison between the conventional PI controller and the proposed Improved Sliding Mode (ISM) controller with PSO-based tuning, evaluated under nominal, stepped, and turbulent wind scenarios. Each metric reflects the average or representative performance across five simulation runs per scenario. The improvement column indicates the relative gain achieved by the ISM controller. Performance metrics demonstrate substantial enhancement in current quality, speed and voltage regulation, torque smoothness, and power quality, with minimal tuning overhead.

In conclusion, the proposed ISM controller with PSO tuning offers substantial performance improvements across dynamic response, signal quality, power regulation, and mechanical stability. These improvements validate the controller’s suitability for advanced WECS applications, addressing both grid compliance and system durability.

7.4. Robustness under extreme wind variations

To evaluate the robustness of the proposed Integral Sliding Mode (ISM) controller under harsher, more realistic operating

Table 2. Comprehensive performance comparison between PI and improved ISM controller (PSO-tuned), evaluated under multiple wind scenarios (nominal, stepped, and turbulent).

Metric	PI controller	ISM controller (PSO-tuned)	Improvement (%)	Test context
THD of stator current (%)	0.9 – 3.0	0.3 – 0.85	~65% average reduction	Nominal + extreme wind
THD of coupling filter current (%)	4.0 – 4.5	3.5 – 4.0	~11% average reduction	Nominal + extreme wind
Speed tracking RMSE (rad/s)	4.28	1.06	75.2% reduction	Nominal wind
Speed tracking RMSE (rad/s, extreme)	4.28	1.41	67.0% reduction	Extreme wind
DC-link voltage RMSE (V)	15.2	4.8	68.4% reduction	Nominal wind
Electromagnetic torque ripple (STD, Nm)	12.4	4.2	66.1% reduction	All wind profiles
Turbine efficiency (C_p)	~0.36 – 0.40	>0.42	~10–15% improvement	Nominal wind
Efficiency at 11 m/s (%)	87.1	93.6	7.5% increase	Steady-state @ 11 m/s
Reactive power at 9 m/s (kVAR)	5.4	2.1	61.1% reduction	Nominal wind
Reactive power at 9 m/s (extreme)	5.4	3.3	38.9% reduction	Extreme wind
PSO convergence time (s)	—	1.2	—	Offline (30 particles)
Chattering impact	Present	Reduced via optimized switching gain	Qualitative	Nominal + extreme wind
Switching loss consideration	Not addressed	Mitigated by smoother torque and lower THD	Qualitative	All wind profiles
Optimization method	Manual tuning	PSO (offline, fast convergence in <32 iter.)	—	Tuning phase (not simulation)

Table 3. Summary of robustness evaluation.

Metric	ISM controller (nominal wind)	ISM controller (extreme wind)	PI controller (nominal wind)
Speed tracking RMSE (rad/s)	1.06	1.41	4.28
Electromagnetic torque ripple (Nm)	± 6	± 9	$> \pm 24$
DC-Link voltage deviation (V)	± 4.8	± 9	± 22
THD of stator current (%)	0.3–0.85	0.4–1.1	0.9–3.0
THD of coupling filter current (%)	3.5–4.0	3.8–4.3	4.0–4.5
Reactive power deviation at 9 m/s (kVAR)	2.1	3.3	5.4

Table 4. Comparative performance metrics of the proposed ISM controller and conventional PI controller during LVRT scenario.

Metric	ISM controller (proposed)	PI controller (conventional)	Improvement
Rotor current overshoot (p.u.)	1.7	2.6	34.6% reduction
DC-link voltage deviation (%)	± 7.4	± 14.8	50.0% reduction
Torque ripple during fault (Nm)	± 9.5	± 18.0	47.2% reduction
Speed deviation during fault (rad/s)	± 2.6	± 5.2	50.0% reduction
Peak reactive power output (kVAR)	+4.1	+2.7	51.8% increase (better support)

conditions, a new simulation scenario was introduced where the wind profile includes sharp gusts and turbulence. This test goes beyond the nominal range (9–12 m/s) and incorporates extreme fluctuations from 6 m/s to 14 m/s. These variations simulate real-world transient phenomena such as sudden wind shear, gusts, and dropouts, allowing us to assess the adaptability and resilience of the control strategy.

A) Wind profile description

Fig. 14 illustrates the modified wind speed profile used in this robustness test. The profile features:

- Sudden wind drop from 12 m/s to 6 m/s (at $t = 3.5$ s)
- Rapid gust up to 14 m/s (at $t = 6.8$ s)
- Return to nominal condition (12 m/s at $t = 9$ s)

These changes occur within milliseconds to seconds, imitating turbulent wind conditions as found in high-altitude or coastal regions.

B) Generator speed response

The generator's response to this challenging wind profile is shown in Fig. 15. The ISM controller maintains tracking accuracy across all wind levels with minimal overshoot or undershoot. During the abrupt wind drop ($t = 3.5$ s), the ISM controller quickly decreases generator speed, avoiding instability. When the wind surges at $t = 6.8$ s, the controller responds within 0.3 seconds, preventing over-acceleration and maintaining smooth convergence to the new reference.

Quantitatively, the Root Mean Square Error (RMSE) of speed tracking in the presence of these disturbances increased only slightly from 1.06 rad/s to 1.41 rad/s, still well below the 4.28 rad/s measured for the PI controller under standard wind changes.

C) Torque, voltage, and power stability (descriptive summary)

Although not shown in figures, the following observations were made from simulation logs:

- Electromagnetic torque remained bounded within ± 9 Nm during wind peaks, up from ± 6 Nm in nominal cases, yet still 60% more stable than the PI controller (which exhibited $> \pm 24$ Nm).

- DC-link voltage saw a maximum deviation of only ± 9 V, compared to ± 4.8 V in stable wind and ± 22 V under PI control, confirming robustness of the GSC regulation.

- Active power delivery adjusted rapidly with the wind changes, and reactive power remained within grid-compliant limits without exceeding ± 4.1 kVAR.

- Total harmonic distortion (THD) of stator and coupling filter currents increased by less than 0.3%, remaining within IEEE 519 standards.

These results suggest that although dynamic performance degrades slightly under extreme wind, the proposed ISM controller retains effective regulation without instability, oscillation, or power quality violations.

D) Discussion

This robustness evaluation demonstrates that the ISM controller, tuned via PSO, maintains satisfactory performance even under severe wind disturbances. The integral sliding surface is used and PSO-tuned gains balance speed tracking and signal smoothness. The offline tuning approach has no limit on online performance in volatile conditions which indicates feasibility for field placement in harsh wind. Despite the minor degradation relative to nominal wind scenarios, the controller remains grid standards, defends mechanical integrity, and continues power delivery. Future enhancement is an adaptive gain scheduling or fuzzy-modulated switching for further enhancement of performance in extreme wind episodes.

Although minor degradation is observed compared to nominal wind scenarios, the controller sustains grid standards, protects mechanical integrity, and ensures continuity of power delivery.

Future improvements could include adaptive gain scheduling or fuzzy-modulated switching to further enhance performance during extreme wind episodes.

7.5. Grid fault ride-through capability

For the evaluation of the dependence of the ISM controller under grid disturbances, for simulation, we used a Low Voltage Ride-Through (LVRT) scenario. This test studies the controller's ability for maintaining operational stability and complying with grid code requirements in a symmetrical voltage sag.

A) Fault scenario description

We used a symmetrical three-phase voltage dip down to 30% of nominal grid voltage at the stator terminals, lasting from $t = 2.5$ s to $t = 3.2$ s (700 ms duration). This is a typical grid fault needing fault ride-through capability. The wind speed stables at at 11 m/s for the isolation of the impact of the grid disturbance aligned with grid code specifications outlined in [1], in which wind turbines stay connected and support grid voltage recovery in short-term voltage dips.

B) Controller response and analysis

Rotor current limitation:

The ISM controller restricts rotor current overshoot to 1.7 p.u., remaining within the safe operational range of the power converter. In comparison, the PI controller results in 2.6 p.u., increasing the risk of overcurrent protection trips.

DC-link voltage stability:

The ISM controller keeps the maximum DC-link voltage deviation within $\pm 7.4\%$ of the nominal 1200 V level, returning to steady-state within 0.4 s after fault clearance. In contrast, the PI controller exhibits a larger deviation of $\pm 14.8\%$, with longer recovery time (~ 1.0 s).

Electromagnetic torque oscillations:

Under ISM control, torque deviations remain bounded within ± 9.5 Nm during the voltage sag. The PI controller experiences wider oscillations, reaching up to ± 18 Nm, which could cause additional mechanical wear.

Speed regulation:

The generator speed deviation during the fault is limited to ± 2.6 rad/s under ISM, whereas the PI controller exhibits deviations of ± 5.2 rad/s, indicating less effective damping.

Reactive power support:

In line with grid code requirements, the ISM controller rapidly increases reactive power output to support voltage recovery, reaching +4.1 kVAR during the fault. The PI controller lags in response, peaking at +2.7 kVAR.

C) Summary of LVRT performance

These results confirm that the proposed ISM controller offers superior performance during grid faults by maintaining current, voltage, and torque within acceptable limits and providing fast, adequate reactive power support. The improved dynamic response and ride-through capability make the controller suitable for deployment in grid-connected wind energy systems subject to modern LVRT requirements. Similar LVRT control strategies for DFIGs have been validated in literature, such as in [41], where fault ride-through performance is emphasized as critical for grid compliance.

8. CONCLUSION

This study improves Integral Sliding Mode (ISM) controller, optimized by the PSO algorithm, developed and tested for a DFIG-based wind energy conversion system. The controller enhanced system performance, reduced chattering, and improved power quality under variable and challenging wind conditions. Simulation results proved the ISM controller and outperformed the traditional PI controller in many aspects. Generator speed tracking accuracy enhanced so much, with a reduction in root mean square error by over 75%. Power quality also saw substantial enhancement, with total harmonic distortion (THD) of the stator current decreased

to less than 0.85%. The controller effectively minimized torque ripple, lowered reactive power consumption at low wind speeds, and increased overall system efficiency to 93.6% at nominal wind conditions. Also, the controller maintained robust performance under extreme wind disturbances, showing strong adaptability and system resilience with no compromising grid standards validating the ISM controller, tuned via PSO, as a practical, efficient, and high-performance solution for modern wind energy systems which supports their reliable integration into renewable energy networks. Future work may involve implementing adaptive or online tuning methods to further improve responsiveness under real-time wind variability. Additionally, experimental validation through hardware-in-the-loop (HIL) testing or field deployment can help assess practical feasibility and long term reliability in actual wind farm environments.

REFERENCES

- [1] D. Emar, M. Ezzat, A. Y. Abdelaziz, K. Mahmoud, M. Lehtonen, and M. M. Darwish, "Novel control strategy for enhancing microgrid operation connected to photovoltaic generation and energy storage systems," *Electron.*, vol. 10, no. 11, p. 1261, 2021.
- [2] M. Aslan, B. Afif, M. Salmi, B. Merabet, M. Berka, and S. Masoud, "Performance enhancement of microgrid systems using backstepping control for grid side converter and mppt optimization," *Sol. Energy Sustain. Dev. J.*, vol. 14, no. 1, pp. 19–41, 2025.
- [3] P. S. Manoj, A. Vijayakumari, and S. K. Kottayil, "Development of a comprehensive mppt for grid connected wind turbine driven pmsg," *Wind Energy*, vol. 22, no. 6, pp. 732–744, 2019.
- [4] J. Mohammadi, S. Vaez-Zadeh, S. Afsharnia, and E. Daryabeigi, "A combined vector and direct power control for dfig-based wind turbines," *IEEE Trans. Sustain. Energy*, vol. 5, no. 3, pp. 767–775, 2014.
- [5] C. Dardabi, A. Djebli, H. Chojaa, H. Aziz, A. Mouradi, M. A. Mossa, and T. A. Alghandi, "Enhancing the control of doubly fed induction generators using artificial neural networks in the presence of real wind profiles," *PLoS One*, vol. 19, no. 4, p. e0300527, 2024.
- [6] Y. Dbaghi, S. Farhat, M. Mediouni, H. Essakhi, and A. Elmoudden, "Indirect power control of dfig based on wind turbine operating in mppt using backstepping approach," *Int. J. Electr. Comput. Eng.*, vol. 11, no. 3, p. 1951, 2021.
- [7] F. Mazouz, S. Belkacem, I. Colak, S. Drid, and Y. Harbouche, "Adaptive direct power control for double fed induction generator used in wind turbine," *Int. J. Electr. Power Energy Syst.*, vol. 114, p. 105395, 2020.
- [8] A. Younesi, S. Tohidi, and M. R. Feyzi, "Fixed switching frequency scheme for current predictive control of dfig," *J. Energy Manage. Technol.*, vol. 6, no. 2, pp. 73–82, 2022.
- [9] A. Younesi, S. Tohidi, and M. R. Feyzi, "Computationally efficient long horizon model predictive direct current control of dfig wind turbines," *J. Oper. Autom. Power Eng.*, vol. 8, no. 2, pp. 172–181, 2020.
- [10] Y. Bostani and S. Jalilzadeh, "A new approach based on wide-area fuzzy controller for damping of sub synchronous resonance in power system including dfig," *J. Oper. Autom. Power Eng.*, vol. 11, no. 1, pp. 61–68, 2023.
- [11] M. Taoussi, M. Karim, B. Bossoufi, D. Hammoui, A. Lagrioui, and A. Derouich, "Speed variable adaptive backstepping control of the doubly-fed induction machine drive," *Int. J. Autom. Control*, vol. 10, no. 1, pp. 12–33, 2016.
- [12] C. Hamid, A. Derouich, M. Taoussi, O. Zamzoum, and A. Hanafi, "An improved performance variable speed wind turbine driving a doubly fed induction generator using sliding mode strategy," in *2020 IEEE 2nd Int. Conf. Electron. Control Optim. Comput. Sci.*, pp. 1–8, IEEE, Dec. 2020.

- [13] T. A. Abderrazak, A. Iliace, B. M. Sofiane, B. R. Ilyas, and H. Hichem, "Transient stability of power in dfig wind farm through resilient with afr, ida-pbc and pid control." unpublished.
- [14] K. Naresh, P. Reddy, and P. Sujatha, "Design and comparison of performance of dfig based wind turbine with pid controller, fuzzy controller, artificial neural network and model predictive controller," *EAI Endorsed Trans. Energy Web*, vol. 9, no. 37, 2021.
- [15] H. Chojaa, A. Derouich, S. E. Chehaidia, O. Zamzoum, M. Taoussi, and H. Elouatouat, "Integral sliding mode control for dfig based wecs with mppt based on artificial neural network under a real wind profile," *Energy Rep.*, vol. 7, pp. 4809–4824, 2021.
- [16] J. Frqvxpswlq and L. Duh, "Welding consumables: State of the art and tendencies of development," 2003.
- [17] A. A. Hossam-Eldin, E. Negm, M. S. Elgamal, and K. M. AboRas, "Operation of grid-connected dfig using spwm-and thipwm-based diode-clamped multilevel inverters," *IET Gener. Transm. Distrib.*, vol. 14, no. 8, pp. 1412–1419, 2020.
- [18] K. Ouari, Y. Belkhier, H. Djouadi, A. Kasri, M. Bajaj, M. Alsharef, and S. Kamel, "Improved nonlinear generalized model predictive control for robustness and power enhancement of a dfig-based wind energy converter," *Front. Energy Res.*, vol. 10, p. 996206, 2022.
- [19] M. Ali, S. M. Amrr, and M. Khalid, "Speed control of a wind turbine-driven doubly fed induction generator using sliding mode technique with practical finite-time stability," *Front. Energy Res.*, vol. 10, p. 970755, 2022.
- [20] Y. Djeriri, "Robust second order sliding mode control of doubly-fed induction generator for wind energy conversion system," *Acta Electrotech. Inform.*, vol. 20, no. 3, pp. 30–38, 2020.
- [21] D. Cherifi, Y. Miloud, and M. Mostefai, "High performance of direct power control for a doubly fed induction generator based on adaptive fuzzy second order sliding mode controller in wind energy conversion system," *Przegl. Elektrotech.*, no. 11, 2023.
- [22] D. Cherifi and Y. Miloud, "Hybrid control using adaptive fuzzy sliding mode control of doubly fed induction generator for wind energy conversion system," *Period. Polytech. Electr. Eng. Comput. Sci.*, vol. 64, no. 4, pp. 374–381, 2020.
- [23] R. Patel, F. Hafiz, A. Swain, and A. Ukil, "Nonlinear rotor side converter control of dfig based wind energy system," *Electr. Power Syst. Res.*, vol. 198, p. 107358, 2021.
- [24] M. Amer, A. Miloudi, and F. Lakdja, "Optimal dtc control strategy of dfig using variable gain pi and hysteresis controllers adjusted by pso algorithm," *Period. Polytech. Electr. Eng. Comput. Sci.*, vol. 64, no. 1, pp. 74–86, 2020.
- [25] A. Younesi, S. Tohidi, and M. R. Feyzi, "An improved long-horizon model predictive control for dfig in wecs with variable sampling-time," *IET Renew. Power Gener.*, vol. 16, no. 3, pp. 517–531, 2022.
- [26] A. Ullah, S. Ullah, T. U. u. Rahman, I. Sami, A. U. u. Rahman, B. Alghamdi, and J. Pan, "Enhanced wind energy conversion system performance using fast smooth second-order sliding mode control with neuro-fuzzy estimation and variable-gain robust exact output differentiator," *Appl. Energy*, vol. 377, p. 124364, 2025.
- [27] B. Ibrahim, H. Abdelkader, M. A. Hartani, and K. Kayisli, "Optimization of sliding mode control for doubly fed induction generator systems using particle swarm and grey wolf algorithms," *Electr. Power Compon. Syst.*, vol. 52, no. 10, pp. 1782–1795, 2024.
- [28] H. Laina, S. Bougdour, B. Sefriti, S. Sefriti, and I. Boumhidi, "Optimal sliding mode control based on particle swarm optimization for wind turbine," in *2024 Sixth Int. Conf. Intell. Comput. Data Sci.*, pp. 1–8, IEEE, 2024.
- [29] P. Parimala and P. N. Babu, "Advanced control and optimization techniques for dfig wind energy systems: A case study using pelican algorithm and ctid-pid controller," *AIP Adv.*, vol. 15, no. 6, 2025.
- [30] G. S. Bruno, D.-E. A. Mansour, A. Nada, and T. F. Megahed, "Hybrid ann-based mppt control for dfig wind systems using type-2 fuzzy logic and super-twisting sliding mode control," *Smart Grids Sustain. Energy*, vol. 10, no. 2, p. 32, 2025.
- [31] H. Itouchene, Z. Boudries, and F. Amrane, "Improved power control based variable speed wind-turbine dfig under hard work conditions: Application of sliding mode theory," *Period. Polytech. Electr. Eng. Comput. Sci.*, vol. 68, no. 4, pp. 392–412, 2024.
- [32] M. Salman, S. A. R. Kashif, M. S. Fakhar, A. Rasool, and A. S. Hussien, "Optimizing power generation in a hybrid solar wind energy system using a dfig-based control approach," *Sci. Rep.*, vol. 15, no. 1, p. 10550, 2025.
- [33] Z. Faramarzi, S. Abazari, S. Houghoughi, and N. Abjadi, "Improved power system dynamic stability by dfig in the presence of sssc using adaptive nonlinear multi-input backstepping," *J. Oper. Autom. Power Eng.*, vol. 12, no. 2, pp. 107–120, 2024.
- [34] Y. Atifi, M. Kissaoui, A. Raihani, K. Errakkas, and A. Khayat, "Advanced nonlinear control of wec system in ac microgrid connected to the main grid with electric vehicle integration," *e-Prime-Adv. Electr. Eng. Electron. Energy*, vol. 9, p. 100718, 2024.
- [35] F. Taibi, O. Benzineb, M. Tadjine, M. S. Boucherit, and M. E. H. Benbouzid, "Hybrid sliding mode control of dfig with mppt using three multicellular converters," in *IFAC Proc. Vol.*, vol. 47, pp. 11659–11666, 2014.
- [36] M. ElAzzaoui, H. Mahmoudi, C. Ed-dahmani, and K. Boudaraia, "Comparing performance of pi and sliding mode in control of grid connected doubly fed induction generator," in *2016 Int. Renew. Sustain. Energy Conf.*, pp. 769–774, IEEE, 2016.
- [37] V. Pande, U. Mate, and S. Kurode, "Discrete sliding mode control strategy for direct real and reactive power regulation of wind driven dfig," *Electr. Power Syst. Res.*, vol. 100, pp. 73–81, 2013.
- [38] A. Achar, Y. Djeriri, H. Benbouhenni, R. Bouddou, and Z. Elbarbary, "Modified vector-controlled dfig wind energy system using robust model predictive rotor current control," *Arab. J. Sci. Eng.*, pp. 1–25, 2024.
- [39] R. Shanmugam, D. K. Sakthivel, A. N. Ramaiah, and S. Ramalingam, "Nonlinear control strategy for dc-link voltage control in a dfig of wecs during 3ϕ grid faults," *IEEE Trans. Ind. Electron.*, vol. 71, no. 10, pp. 12468–12475, 2024.
- [40] A. El Ouali, Y. Lakhali, M. Benchagra, H. Chojaa, M. V. O. Mohamed, A. Maarif, and M. A. Mossa, "Comparative study of linear and nonlinear controllers for dfig-based wind power systems under different operating conditions," *J. Rob. Control*, vol. 6, no. 3, pp. 1208–1215, 2025.
- [41] M. J. Hossain, T. K. Saha, N. Mithulananthan, and H. R. Pota, "Control strategies for augmenting lVRT capability of dfigs in interconnected power systems," *IEEE Trans. Ind. Electron.*, vol. 60, no. 6, pp. 2510–2522, 2012.